Computational Materials Science 125 (2016) 82–91

Contents lists available at ScienceDirect

Computational Materials Science

journal homepage: www.elsevier.com/locate/commatsci

Editor's Choice

High-throughput prediction of finite-temperature properties using the quasi-harmonic approximation

Pinku Nath [a], Jose J. Plata [a], Demet Usanmaz [a], Rabih Al Rahal Al Orabi [b], Marco Fornari [b], Marco Buongiorno Nardelli [c], Cormac Toher [a], Stefano Curtarolo [a,*]

[a] Department of Mechanical Engineering and Materials Science, Duke University, Durham, NC 27708, USA
[b] Department of Physics and Science of Advanced Materials Program, Central Michigan University, Mount Pleasant, MI 48858, USA
[c] Department of Physics and Department of Chemistry, University of North Texas, Denton TX, USA

ARTICLE INFO

Article history:
Received 23 June 2016
Received in revised form 25 July 2016
Accepted 28 July 2016
Available online 6 September 2016

Keywords:
High-throughput
Materials genomics
Quasi-harmonic approximation
AFLOW

ABSTRACT

In order to calculate thermal properties in automatic fashion, the Quasi-Harmonic Approximation (QHA) has been combined with the Automatic Phonon Library (APL) and implemented within the AFLOW framework for high-throughput computational materials science. As a benchmark test to address the accuracy of the method and implementation, the specific heat capacities, thermal expansion coefficients, Grüneisen parameters and bulk moduli have been calculated for 130 compounds. It is found that QHA-APL can reliably predict such values for several different classes of solids with root mean square relative deviation smaller than 28% with respect to experimental values. The automation, robustness, accuracy and precision of QHA-APL enable the computation of large material data sets, the implementation of repositories containing thermal properties, and finally can serve the community for data mining and machine learning studies.

1. Introduction

The characterization and prediction of thermal properties of materials are among the key factors enabling a rational accelerated materials development [1]. Important properties include specific heat capacity at constant volume/pressure (C_V or C_p), mode resolved and average Grüneisen parameters (γ_{qj} and γ), thermal expansion coefficient (α_V), Debye temperature (θ_D), lattice thermal conductivity (κ_l), and vibrational entropy and Gibbs free energy ($S(p,T)$ and $G(p,T,V)$).

There are several computational techniques leading to the characterization of these thermal properties: **i.** First principles molecular dynamics (extremely time consuming and computationally impractical for creating large datasets). **ii.** The GIBBS approach [2] also implemented in the AFLOW-AGL (Automatic-Gibbs-Library) [3] (very fast and reasonably reliable especially for high-throughput screening [1]). **iii.** Anharmonic force constant calculations and Boltzmann Transport Equation solvers, as implemented in ShengBTE [4], PHONO3PY [5] and in the AFLOW-APL2 Library [6] (computationally intensive but capable of giving very accurate values for κ_L). **iv.** Approaches based on the QHA [7–14] which can rapidly characterize C_V, C_p, γ, and α_V. Methods **ii.–iv.** are based on phonon calculations as available in packages like AFLOW-APL [15,16], PHONOPY [17], Phon [10], and ALAMODE [18].

With the goal of creating large repositories of *ab initio* calculated properties, such as in our AFLOW.org [19–21] online database, we have undertaken the task of implementing the quasi-harmonic method in the AFLOW software platform [15]. The quasi-harmonic method is based on the construction of a strain dependent free energy function in which each strained structure belongs to the harmonic regime. The strain dependent free energy contributes as a vibrational energy and introduces anharmonic effects into the system, including the temperature dependence. Although this method has been successfully applied for decades, it has limitations: the QHA loses predictive power when anharmonic forces play a major role in the dynamics (as in the case of thermal conductivity), under extreme conditions in term of temperature and pressure [22,23] or close to their melting point [24]. Despite these limitations, this model has been satisfactorily demonstrated to accurately and robustly predict many temperature-dependent properties for compounds of different nature [25–32].

Even if the QHA is a well-established approach, its implementation within an automatic framework requires addressing several challenges. Therefore, despite the availability of the previously

* Corresponding author.
E-mail address: stefano@duke.edu (S. Curtarolo).

http://dx.doi.org/10.1016/j.commatsci.2016.07.043
0927-0256/

mentioned packages (PHONOPY and ALAMODE), to the best of our knowledge, there is not yet a high-throughput [1] framework able to predict temperature dependent properties using the QHA in a self-contained robust way. The high-throughput protocol should include: automatic generation of files, robust correction of errors and post-processing, and appropriate interface to a material database [19]. In this article, we show tests of our QHA implementation in AFLOW by computing temperature dependent thermodynamic properties for more than one hundred materials. For one case we assess the effect of improved electronic structure [33] on the thermal properties.

2. Methods

2.1. Ab initio thermodynamics

In the framework of the QHA, the Helmholtz free energy, F, for a fixed number of particles, is written as

$$F(V,T) = E_{0K}(V) + F_{vib}(V,T) + F_{elec}(V,T) \tag{1}$$

where E_{0K} is the total energy of the system at 0 K and given volume, V. F_{vib} represents the vibrational contribution to the free energy and F_{elec} is the electronic contribution to the free energy as function of volume and temperature. The total energy at any volume and 0 K can be computed by using standard periodic quantum mechanical software such as Quantum Espresso [34] or the Vienna Ab-initio Simulation Package (VASP) [35] and properly relaxed structures. The vibrational free energy, which includes zero point energy contributions, can be obtained from the phonon density of states, $g(\nu)$, via:

$$F_{vib}(V,T) = \int_0^\infty g(\nu)\left[\frac{h\nu}{2} + k_B T \ln\left(1 - \exp\left(-\frac{h\nu}{k_B T}\right)\right)\right] d\nu \tag{2}$$

where k_B, h, and ν are the Boltzmann constant, the Planck constant, and the vibrational frequency respectively. Frequencies for a given wave vector $\mathbf{q}$ can be computed by diagonalizing the dynamical matrix. The phonon density of states, pDOS, can be computed by integrating the phonon dispersion in the Brillouin zone.

Similarly, F_{elec}, can be computed as:

$$F_{elec}(V,T) = \Delta E_{elec}(V,T) - TS_{elec}(V,T) \tag{3}$$

where $\Delta E_{elec}(V,T)$ and $S_{elec}(V,T)$ are the contribution to the electronic energy due to temperature changes and the electronic entropic contribution to the free energy. At low temperatures, $\Delta E_{elec}(V,T)$ is very small and can be neglected. However, it may play a significant role at high temperatures. Both can be computed using the electronic density of states, eDOS,

$$\Delta E_{elec}(V,T) = \int n(\epsilon) f \epsilon d\epsilon - \int^{\epsilon_F} n(\epsilon)\epsilon d\epsilon \tag{4}$$

$$S_{elec}(V,T) = -k_B \int n(\epsilon)[f \ln f + (1-f)\ln(1-f)] d\epsilon \tag{5}$$

where the eDOS at energy, ϵ, is represented by $n(\epsilon)$, and f is the Fermi distribution function.

Once $F(V,T)$ is computed at different volumes and temperatures, extracting the thermodynamic data is a straightforward process using the equations of state. For instance, properties like equilibrium free energy, F_{eq}, equilibrium volume, V_{eq}, bulk modulus, B, and the derivative of the bulk modulus with respect to pressure, B_p, can be obtained by fitting $F(V,T)$ at different volumes and temperatures to the Birch-Murnaghan (BM) function:

$$F(V) = F_{eq} + \frac{BV_{eq}}{B_p}\left[\frac{(V_{eq}/V)^{B_p}}{Bp-1} + 1\right] - \frac{V_{eq}B}{Bp-1} \tag{6}$$

where F_{eq}, B, V_{eq} and B_p are used as the fitting parameters.

The mode Grüneisen parameters, γ_{qj}, for the wave vector $\mathbf{q}$ and the phonon branch j can be computed by taking the derivative of the dynamical matrix with respect to the volume, as [36]:

$$\gamma_{qj} = -\frac{V_{eq}^{0K}}{2\nu_{qj}^2}\sum_j e_{qj}\frac{\partial D_q}{\partial V}e_{qj}^* \tag{7}$$

where D_q is the dynamical matrix for a wave-vector, $\mathbf{q}$, ν_{qj} vibrational frequency, and e_{qj} is the eigenvector for phonon branch, j. An average Grüneisen parameter, $\gamma(T)$, can be obtained using [37,38]:

$$\gamma(T) = \frac{\sum_{qj}\gamma_{qj}C_{V_{qj}}}{C_V} \tag{8}$$

where $C_{V_{qj}}$, is the isochoric specific heat:

$$C_{V_{q,j}} = k_B\sum_{q,j}\frac{(h\nu_{qj}^2)\exp(h\nu_{qj}/k_BT)}{(k_BT)^2(\exp(h\nu_{qj}/k_BT)-1)^2} \tag{9}$$

Once $\gamma(T)$ is calculated, other variables such as volumetric thermal expansion $\alpha_V(T)$ and isobaric specific heat, C_p can be predicted using Eqs. (10) and (11) respectively:

$$\alpha_V(T) = \frac{C_V(T)\gamma(T)}{V(T)B(T)} \tag{10}$$

$$C_p - C_V = \alpha^2(T)B(T)V(T)T \tag{11}$$

2.2. Computational details

In the QHA-APL we first perform a geometry optimization minimizing the forces acting on the atoms in the primitive cell and the stresses. The optimized geometry is used as starting point for the other calculations. The phonon dispersions are computed at three different volumes to determine the Grüneisen parameters, one at the equilibrium volume and the other two at slightly distorted volumes (less than ±5% of the volume). Finally, the data are used to fit the BM equation of state. These calculations are automatically generated, managed and monitored by the AFLOW [15,20] package, facilitating and accelerating the prediction of all properties required by the user in the original input.

2.2.1. Geometry optimization

All structures are fully relaxed using the HT framework, AFLOW [15], and the DFT Vienna Ab-initio simulation package, VASP [35]. Optimizations are performed following the AFLOW standards [21]. We use the projector augmented wave (PAW) pseudopotentials [39] and the exchange and correlation functionals parametrized by the generalized gradient approximation proposed by Perdew-Burke-Ernzerhof (PBE) [40]. All calculations use a high energy-cutoff, which is 40% larger than the maximum recommended cutoff among all component potentials, and a k-points mesh of 8000 k-points per reciprocal atom. Primitive cells are fully relaxed (lattice parameters and ionic positions) until the energy difference between two consecutive ionic steps is smaller than 10^{-4} eV and forces in each atom are below 10^{-3} eV/Å.

2.2.2. Phonon calculations

Phonon calculations were carried out using the automatic phonon library, APL, as implemented in the AFLOW package, using VASP to obtain the interatomic force constants (IFCs) via the finite-displacement approach. The magnitude of this displacement is 0.015 Å. Non-analytical contributions to the dynamical matrix are also included using the formulation developed by Wang et *al.*

[41]. Frequencies and other related phonon properties are calculated on a 21 × 21 × 21 mesh in the Brillouin zone, which is sufficient to converge the vibrational density of states, pDOS, and hence the values of thermodynamic properties calculated through it. The pDOS is calculated using the linear interpolation tetrahedron method available in AFLOW package. The derivative of dynamical matrix in Eq. (7) is obtained using the central difference method within a volume range of ±0.03%.

In order to balance accuracy and computational cost, the dimension of the supercell for IFCs calculations has been optimized. Since the average Grüneisen parameter is an important variable in our equations, we have evaluated this property for different cell size for Si. Results and comparison with experimental results are shown in Fig. 1. We note that a 3 × 3× 3 supercell, containing 54 atoms, predicts almost the same quantitative values as the 4 × 4× 4 supercell (128 atoms) in the 100–700 K range, while dramatically reducing the number of atoms and computational time. Therefore, we have built supercells with at least 27 atoms per reciprocal atom in the primitive cell homogeneously distributed in all directions.

2.2.3. Distorted volume single point calculations

To obtain $F(V,T)$ vs. $V(T)$ curves, phonon calculations have been performed for thirteen equally spaced configurations in which the volume of cell was compressed and expanded in the range from 98% to 104% of its fully relaxed value. $F_{elec}(V,T)$ is computed from static and band calculations of the expanded and compressed primitive cells following AFLOW standard [21] that are consistent with the setup used for the geometry optimizations.

There are limitations derived by the level of theory or functional. PBE could predict metallic behavior in semiconductors with a narrow band gap. This error would modify $F_{elec}(V,T)$ which is a small contribution at low and moderate temperatures. To verify that none of the materials included in the data set present this anomaly, we have compared the calculated band gaps with the experimental values (see Table 1 in Supplementary Information).

2.3. Analysis of results

Different statistical parameters have been used to measure the qualitative and quantitative agreement of QHA-APL with experimental values. The Pearson correlation coefficient r is a measure of the linear correlation between two variables, X and Y. It is calculated by

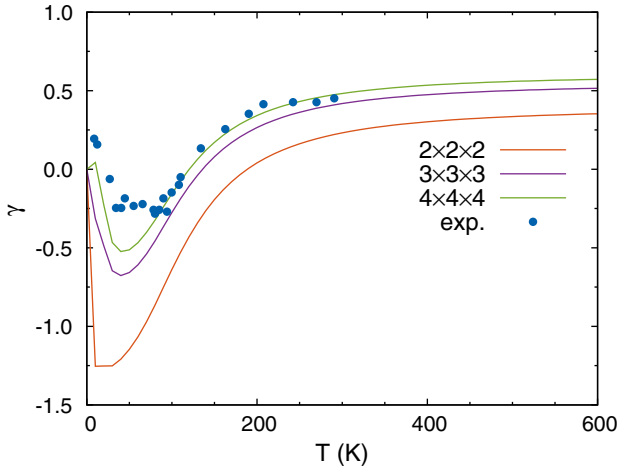

Fig. 1. Average Grüneisen parameter for three different super-cell sizes for Si. Circles represent experimental values [42].

$$r = \frac{\sum_{i=1}^{n}(X_i - \overline{X})(Y_i - \overline{Y})}{\sqrt{\sum_{i=1}^{n}(X_i - \overline{X})^2}\sqrt{\sum_{i=1}^{n}(Y_i - \overline{Y})^2}}, \tag{12}$$

where X and Y are the mean values of X and Y.

The Spearman rank correlation coefficient ρ is a measure of the monotonicity of the relationship between two variables. The values of the two variables X_i and Y_i are sorted in ascending order, and are assigned rank values x_i and y_i which are equal to their position in the sorted list. The correlation coefficient is then given by

$$\rho = \frac{\sum_{i=1}^{n}(x_i - \overline{x})(y_i - \overline{y})}{\sqrt{\sum_{i=1}^{n}(x_i - \overline{x})^2}\sqrt{\sum_{i=1}^{n}(y_i - \overline{y})^2}}. \tag{13}$$

It is useful for determining how well the ranking order of the values of one variable predict the ranking order of the values of the other variable.

We also investigate the root-mean-square relative deviation (RMSrD) of the calculated results from experiment. This gives a measure of the magnitude of the difference between the QHA-APL predictions and experiment. The root mean square relative deviation (RMSrD) is calculated using the expression

$$\mathrm{RMSrD} = \sqrt{\frac{\sum_{i=1}^{n}\left(\frac{X_i - Y_i}{X_i}\right)^2}{n-1}}, \tag{14}$$

Note that lower values of the RMSrD indicate better agreement with experiment.

3. Results

A benchmark of 130 materials has been used to demonstrate the accuracy and robustness of this method (see Table 1). To maximize the heterogeneity of the data set, these compounds were selected to belong to different crystallographic lattices (cubic, tetragonal, orthorhombic, hexagonal, rhombohedral and monoclinic) as well as different electronic properties (insulators, semiconductors and metals, see Supplementary Information for the computed and experimental energy gaps).

For each temperature, we calculated the free energy (F) at different volumes (V). These F vs. V curves are initially fitted to a cubic function which is used as an initial guess to fit the Birch-Murnaghan equation of state (see Section 2 and Eq. (6)). As an example, the results of the final fitting for Si are depicted in Fig. 2. Automatic tests to ensure the correct fitting of the curves have been implemented to warn of possible errors, especially in magnetic systems or close to phase transition temperatures. The bulk modulus, B, at 300 K is obtained by the fitting procedure. Fig. 3(a) illustrates the distribution of B for the whole set of materials while Fig. 3(b) compares experimental and predicted values of B for those materials with available experimental data. The computed values range over two orders of magnitude, from C diamond (442 GPa) to K (3.2 GPa). To quantify the accuracy, precision and robustness of our results we have used different statistical quantities such as mean absolute deviation (MAD), root mean square deviation (RMSD), root mean square relative deviation (RMSrD), relative maximum absolute deviation (rMAX), and Pearson and Spearman correlation (see Table 2). Most of the predicted values are within a 20% error (dashed lines in Fig. 3(b)), presenting a RMSrD of around 17% and a rMAX close to 22.9%. Values close to 1.0 for the Pearson and Spearman correlations also demonstrate that our implementation of the QHA is robust and that the results can be compared with experimental data.

In the spirit of the QHA, the Grüneisen parameter, $\gamma(T)$, is often used to estimate the anharmonicity of the vibrations in the crystal. Methods such as AGL are able to predict reasonably accurate values

Table 1
ICSD identification number, Bulk modulus (B), Grüneisen parameter (γ), Volumetric thermal expansion coefficient (α), and Isochoric specific heat (C_p) for material data set. Experimental values in parenthesis. Units: B in GPa, α in 10^{-6} K^{-1}, and C_p in J mol^{-1} K^{-1} (see Supplementary Information for the computed and experimental energy gaps).

Formula	ICSD	B	γ	α	C_p	Formula	ICSD	B	γ	α	C_p
Ag_1Cl_1	157535	28.6(44.0) [43]	2.30	114.0	53.5(53.0) [44]	Ge_1	44841	55.1(78.0) [45]	0.74(0.76) [46]	21.5(16.2) [47]	23.3(23.3) [44]
Ag_1Mg_1	184,205	48.6	2.14	89.2	50.5	Ge_1Mg_2	81,735	46.63	1.46	53.8	71.2
Ag_1Sc_1	58,348	65.8	1.66	46.6	49.3	H_1Li_1	61,751	32.0(33.7) [48]	1.10(1.28) [46]	87.1	27.6(28.1) [44]
Ag_3Mg_1	58,323	58.1	2.41	86.9	102.7	$H_1Li_1Pd_1$	246,613	77.5	1.71	63.4	17.7
Al_1As_1	606,008	64.5(77.0) [49]	0.57(0.66) [46]	13.7	44.4(45.8) [44]	$H_1Mg_1Ni_1$	187,257	86.3	1.21	40.1	55.1
Al_1B_2	159,334	167.5	1.16	22.2	51.0(43.9)	H_1Na_1	183,291	18.8	0.79	78.9	34.8(36.5)
Al_1	240,129	67.5	2.41	80.8(69.0) [47]	24.3(24.2) [47]	H_1Ti_1	168,325	112.8	0.88	15.8	26.4
Al_1Li_1	240121	47.6	1.54	69.1	44.5(48.9) [44]	Hg_1Ni_1	639119	104.8	2.82	68.2	51.3
Al_1N_1	602,459	188.0(201.0) [50]	0.80(0.70) [51]	10.1	31.0(30.1) [44]	Hg_1Pd_1	639,137	101.0	3.10	67.2	52.0
Al_1Ni_1	608,805	147.1	1.93	40.5	45.9(45.9) [44]	Hg_1Pt_1	104,337	127.4	3.28	57.0	51.8
Al_1P_1	609,019	80.6(86.0) [49]	0.50(0.75) [51]	10.3	41.5(42.0) [44]	Hg_1Zr_1	639,318	97.6	2.19	41.3	49.9
Al_1Sb_1	609,290	47.3(58.2) [45]	0.44(0.60) [46]	11.7(12.6) [47]	45.8	I_1K_1	53,827	8.3(11.1) [52]	1.77(1.45) [46]	178.6(122.4) [53]	54.0(52.80) [53]
Al_1Sc_1	58,098	63.6	1.83	52.9	47.0	I_1Li_1	27,983	9.7	2.93	395.9(178.2) [53]	65.1
$Al_1Si_1Sr_1$	162,865	51.9	1.31	37.7	69.3	I_1Na_1	52,240	14.0(15.95) [52]	1.94(1.56) [46]	156.0(136.5) [53]	53.5(52.26) [53]
Al_1Tb_3	58,173	45.9	0.51	16.2	96.5	I_1Rb_1	53,846	7.1(11.1) [52]	1.54(1.41) [46]	161.6(124.5) [53]	53.3(52.5) [44]
Al_1Ti_1	187,030	92.1	1.54	35.6	45.6(49.3) [44]	In_1N_1	157,515	118.5(126.0) [54]	0.82(0.97) [55]	14.3	40.0
Al_3Ti_1	609,525	97.9	1.49	33.8	89.7	In_1P_1	165,466	56.5(71.0) [49]	0.62(0.60) [46]	15.7(13.8) [47]	45.6(45.5) [44]
As_1B_1	181,292	126.6	0.80	13.0	34.9	In_1Te_1	169,431	34.0	2.57	96.1	52.9(47.7) [44]
$As_1Ba_1Li_1$	56,445	31.1	1.27	55.7	70.9	In_1Te_1	640,622	32.3	2.57	101.1	53.1(47.7) [44]
As_1Ga_1	53,964	57.2(74.8) [49]	0.76(0.75) [46]	21.6(16.2) [47]	46.9(46.8) [44]	K_1	641,218	2.6(3.1)	0.80	158.2	25.7(29.4) [44]
As_1In_1	165,462	43.6(58.0) [49]	0.64(0.57) [46]	19.7(14.1) [47]	43.6(47.8) [44]	K_2O_1	44,674	45.1	1.76	73.7	73.7
B_1Sb_1	184,571	94.9	0.85	15.2	38.0	K_2S_1	183,837	35.9	1.54	50.0	74.3
B_2Ti_1	78,847	231.4	1.27	15.3	45.7	Li_1Pd_1	642,257	52.5	1.62	80.9	45.5
B_2V_1	167,794	265.9	1.35	15.8	45.8	Li_1Pt_1	104,777	110.2	1.44	34.1	44.5
Be_1	52,708	99.4	1.63	54.2	16.5(16.52) [44]	Li_2O_1	60,431	72.8(88.0)	1.19	55.1	53.9
Be_1Rh_1	58,734	210.0	2.10	32.5	43.1	Li_2S_1	657,596	31.3	1.22	83.3	64.4
Be_1S_1	186,889	89.7(105.0) [56]	0.91	20.9	36.7(34.2) [44]	Li_2Se_1	168,446	28.4	1.04	70.7	66.8
Be_1Se_1	616,419	70.8(92.0) [56]	0.80	21.1	39.9	Li_2Te_1	642,399	24.0	1.06	69.4	69.0
Be_1Te_1	290,008	53.8(67.0) [56]	0.72	19.9	41.6	Mg_1O_1	159,372	147.3(164) [57]	1.53(1.44) [46]	33.3	38.3(37.2) [44]
Be_2C_1	616,184	179.3	1.17	20.2	38.9(43.3) [44]	Mg_1Pt_3	104,857	164.1	2.70	40.1	98.4
Bi_1Na_1	616,837	24.1	1.92	106.8	51.9	Mg_1S_1	53,939	68.1	1.68	50.7	46.4(45.6) [44]
Br_1Cu_1	30,090	36.8	1.19	53.5(46.2) [47]	49.5(54.8) [44]	Mg_1Sc_1	108,583	48.1	1.56	51.3	47.8
Br_1K_1	52,243	11.0(15.4) [52]	1.87(1.45) [46]	170.5(116.1) [53]	53.7(52.3) [53]	Mg_1Se_1	159,398	53.3	0.27	71.8	46.2 (48.0)
Br_1Li_1	53,819	19.4(26.0) [52]	2.39	216.6(149.4) [53]	54.9(48.9) [53]	Mg_2Pb_1	104,846	29.9	1.27	59.4	73.1(72.5) [44]
Br_1Na_1	44,278	16.0(19.6) [52]	1.69(1.5) [46]	148.0(126.9) [53]	52.3(51.9) [53]	Mg_2Si_1	163,708	17.0	1.22	44.3(34.5) [47]	68.7(68.0) [44]
C_1	182,729	416.9(442.0) [45]	0.73(0.75) [46]	3.2(3.5) [47]	6.4 (8.6) [44]	Mg_2Sn_1	151,368	37.8	1.30	50.0(29.7) [47]	72.3
C_1Si_1	618,777	211.0(211.0) [45]	0.72(0.75) [46]	7.3	27.7(27.1) [44]	Mn_1O_1	18,006	136.3	1.78	39.9	44.1(44.17) [44]
C_1Ti_1	181,681	230.0	1.44	16.8	35.1(33.9) [44]	Mn_1S_1	76,205	52.9	0.42	12.8	45.9(45.6) [44]
C_1Zr_1	180,599	212.0	1.58	17.9	38.7	Mn_1Se_1	24,252	45.0	0.30	9.7	47.6(51.0) [44]
Ca_1Cd_1	619,188	27.3	1.57	78.6	50.4	Mn_1Te_1	181,324	68.9	0.23	7.9	48.3
Ca_1F_2	40,938	68.3(84.0)	1.78	68.7	68.7(68.7) [44]	N_1Sc_1	155,049	179.2	1.57	22.7	38.6

(*continued on next page*)

Table 1 (*continued*)

Formula	ICSD	*B*	γ	α	C_p	Formula	ICSD	*B*	γ	α	C_p
Ca_1O_1	180,198	98.6(113) [58]	1.57(1.57) [46]	39.3	43.4(42.2) [44]	N_1Ti_1	183,415	248.3	1.71	21.0	37.6(37.2) [44]
Ca_1S_1	619,530	69.6	1.46	34.1	47.0(47.4) [44]	Na_1	644,903	6.7	1.32	20.3	26.4
Ca_1Se_1	619,570	46.0	1.50	47.8	48.8(48.1) [44]	Se_1Zn_1	181,761	53.3	0.83	26.4	47.8
Ca_1Te_1	619,616	34.6	1.47	51.3	49.5(41.6) [44]	Ni_1O_1	166,115	168.9	1.59	33.6	42.1(44.5) [44]
Cd_1F_2	28,864	79.3	2.20	74.1	71.2	Ni_1Sb_1	646,431	107.3	1.73	36.2	48.6
Cd_1O_1	181,735	114.4	1.94	46.0	46.1(43.7) [44]	Ni_1Sc_1	105,333	96.2	1.86	45.6	48.7
Cd_1Pd_1	620,270	91.6	2.32	57.1	50.4	Ni_1Zn_1	647,134	129.5	1.86	46.8	48.1
Cd_1Pt_1	620,297	119.3	2.70	51.7	50.7	$Ni_2Sn_1Ti_1$	646,777	138.5	2.17	41.3	97.2(98.0) [44]
Cd_1S_1	290,009	46.8	0.53(0.75) [51]	16.8	46.7	O_1Pd_1	26,598	142.3	1.51	19.8	39.1
Cd_1Sr_1	102,066	19.8	1.51	89.0	51.3	O_1Sr_1	26,960	76.4(91.2) [58]	1.63(1.52) [46]	44.8	46.2(45.4) [44]
Cd_3Zr_1	102,093	71.8	1.99	50.5	100.2	O_1Zn_1	182,356	121.0	0.66(0.75) [51]	15.7	40.3(41.17) [44]
Cl_1Cu_1	78,270	35.6	0.86	46.2(36.3) [47]	48.3(52.6) [44]	O_1Zn_1	647,683	121.4(143) [45]	0.66	15.7	40.3
Cl_1K_1	240,522	13.3(18.2) [52]	1.77(1.45) [46]	157.4(111.3) [53]	52.7(51.7) [53]	Pd_1Zn_1	649,134	115.0	2.43	58.4	50.0
Cl_1Li_1	26,909	38.9(32.9) [52]	2.71	119.6(131.4) [53]	50.0(48.1) [53]	Pt_1Zn_1	105,852	159.4	2.13	37.6	49.2
Cl_1Na_1	240,600	19.7(25.1) [52]	1.75(1.56) [46]	145.7(119.1) [53]	51.6(50.54) [53]	S_1Zn_1	108,733	65.6(71.4) [49]	0.79(0.75) [46]	23.1	45.5
Cl_1Rb_1	18,016	10.2(16.2) [52]	1.55(1.45) [46]	156.5(108.0) [53]	52.6(52.3) [53]	Sc_1	164,093	52.1	1.10	30.8	23.8(25.58) [44]
Cu_1I_1	163,427	18.9	1.36	101.0	51.0	Sc_1Zn_1	106,041	65.1	1.39	42.3	48.3
Cu_1	627,117	114.5	1.91	53.5	24.3(24.5) [44]	Si_1	76,268	84.9(100.0) [45]	0.42(0.56) [51]	8.0(7.8) [47]	20.0(20.0) [44]
Cu_1Sn_1	629,278	54.7	2.40	85.4	51.9	Tc_1V_1	106,143	232.5	1.91	21.7	45.9
$Cu_2Ni_1Zn_1$	103,079	124.7	1.93	50.5	96.7	Te_1Zn_1	184,485	39.4(51.0) [49]	0.89(0.97) [46]	30.7	48.6
F_1K_1	52,241	22.5(31.6) [52]	1.59(1.5) [46]	133.4(104.4) [53]	50.5(49.0) [53]	Te_1Zr_1	653,209	93.1	1.60	27.6	48.2
F_1Li_1	53,839	55.8(76.0) [52]	1.63(1.5) [46]	109.9(99.6) [53]	42.8(42.0) [53]	Ti_1	168,830	109.3	1.62	30.1	23.5(25.1) [44]
F_1Na_1	52,238	37.3(48.5) [52]	1.52(1.5) [46]	113.7(95.1) [53]	47.8(46.9) [53]	Zn_1	181,734	44.8	2.47	144.8	26.8(25.41) [44]
Ga_1P_1	77,088	74.8(88.7) [49]	0.70(0.75) [46]	16.2(15.9) [47]	44.1(44.2) [44]	Zn_1Zr_1	181,290	96.3	1.42	31.2	48.3
Ga_1Sb_1	41,675	42.7(45.1) [49]	0.71(0.75) [46]	21.9	47.9						

for the Debye temperature or *B* but fail to predict $\gamma(T)$ [3]. Our QHA-APL results are shown in Fig. 3 which includes, for comparison, the available results using AGL for the same compounds. Despite the higher computational cost of the QHA compared to the AGL methodology (one or two orders of magnitude higher than AGL depending on the size of the system), it is clear that results are tremendously improved. The MAD for QHA-APL is 0.13 for a property whose highest measured value is around 3 and the average values are between 1 and 2. Relative statistical indicators also demonstrate the high accuracy of the method obtaining a RMSrD below 16% and a rMAX lower than 29%. Values larger than 3 are especially interesting for their potential application as thermoelectrics. As we mentioned, $\gamma(T)$ is related to the anharmonicity of the crystal, so high values for this property usually [59] indicate lower values of the lattice thermal conductivity, κ_L, which increases the thermoelectric figure of merit, *ZT*. We have found two materials with γ over 3, however both are metals (HgPd, HgPt). We have looked for other possible candidates with high values of γ considering also that for a high thermoelectric figure of merit they should be semiconductors. K_2O and MnO are the best two candidates, with γ around 1.8 and band gaps below 2 eV. There is no experimental data available for K_2O, although Gheribi et *al.* have predicted a lattice thermal conductivity for this material below 2 W m^{-1} K^{-1} [60].

The Grüneisen parameters for each vibrational mode, γ_{iq}, provide even more information than γ about the anharmonicity of the crystal and the lattice thermal conductivity. High and low values of κ_L in an insulator are usually linked to low and high values of γ_{iq} at low frequency. CSi (κ = 360 W m^{-1} K^{-1}) [51] and NaI (κ=1.8 Wm^{-1}K^{-1}) [51] are two good examples of this trend (see Fig. 4(a) and (b)) that has been exploited in the literature to pinpoint anharmonic effects [61,62]. We have studied the mode Grüneisen parameters of two other materials included in the benchmark whose κ_L has not been measured experimentally. We have already discussed the probable low thermal conductivity of K_2O which is in agreement with the very high mode Grüneisen parameter values at low frequencies (see Fig. 4(d)). BeTe shows the opposite behavior to K_2O, presenting low values for γ_{iq} at low frequencies (see Fig. 4(c)). This trend is in agreement with the AGL prediction of κ_L for BeTe, which is close to the value obtained for AlAs (κ = 98 W m^{-1} K^{-1}) [51]. These predictions validate the use of γ and γ_{iq} as a simple predictors for κ_L and demonstrates that

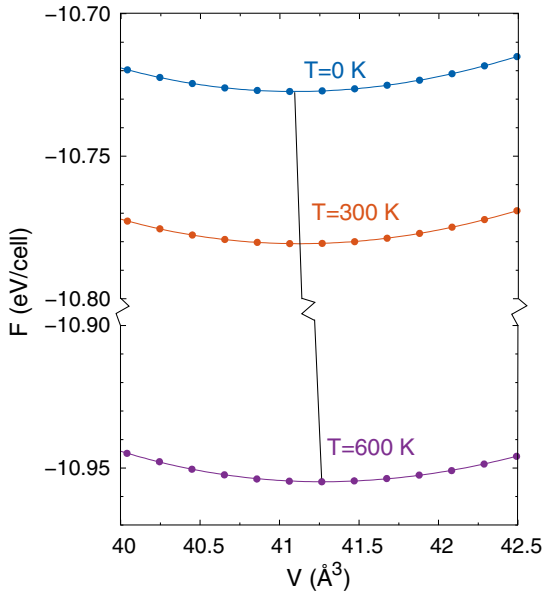

Fig. 2. Free energy and volume data fitted using Birch-Murnaghan function for different temperatures for Si. Points represent calculated data and solid lines indicate the fitted function. Equilibrium volumes at each temperature are connected by solid black line.

Table 2
Mean absolute deviation (MAD), root mean square deviation (RMSD), root mean square relative deviation (RMSrD), relative maximum absolute deviation (rMAX), and Pearson and Spearman correlation for the material data set. Units: MAD and RMSD in the same units that are used in Table 1.

	B	γ	α	C_p
MAD	11.09	0.13	20.22	1.63
RMSD	12.89	0.17	28.15	2.45
RMSrD	17.38%	15.00%	28.0%	6.35%
rMAX	22.9%	28.32%	46.5%	18.9%
r	0.996	0.969	0.974	0.985
ρ	0.990	0.891	0.927	0.929

the QHA-APL method can be used as a powerful method for the discovery of new interesting properties in well known materials.

The volumetric thermal expansion, $\alpha_V(T)$, has very important implications in engineering. However, it is not easy to predict accurately from first principles. Statistical parameters prove again that QHA-APL methodology is a reliable method to obtain this thermodynamic quantity. The uncertainty as described by RMSrD is below 28% and MAD is around $20.22 \times 10^{-6}\,K^{-1}$ for the benchmark in which the range varies between 0 and $160 \times 10^{-6}\,K^{-1}$. Low thermal expansion coefficient materials deserve special attention because they are particularly interesting for a variety of applications. There are 5 materials in our benchmark that present a

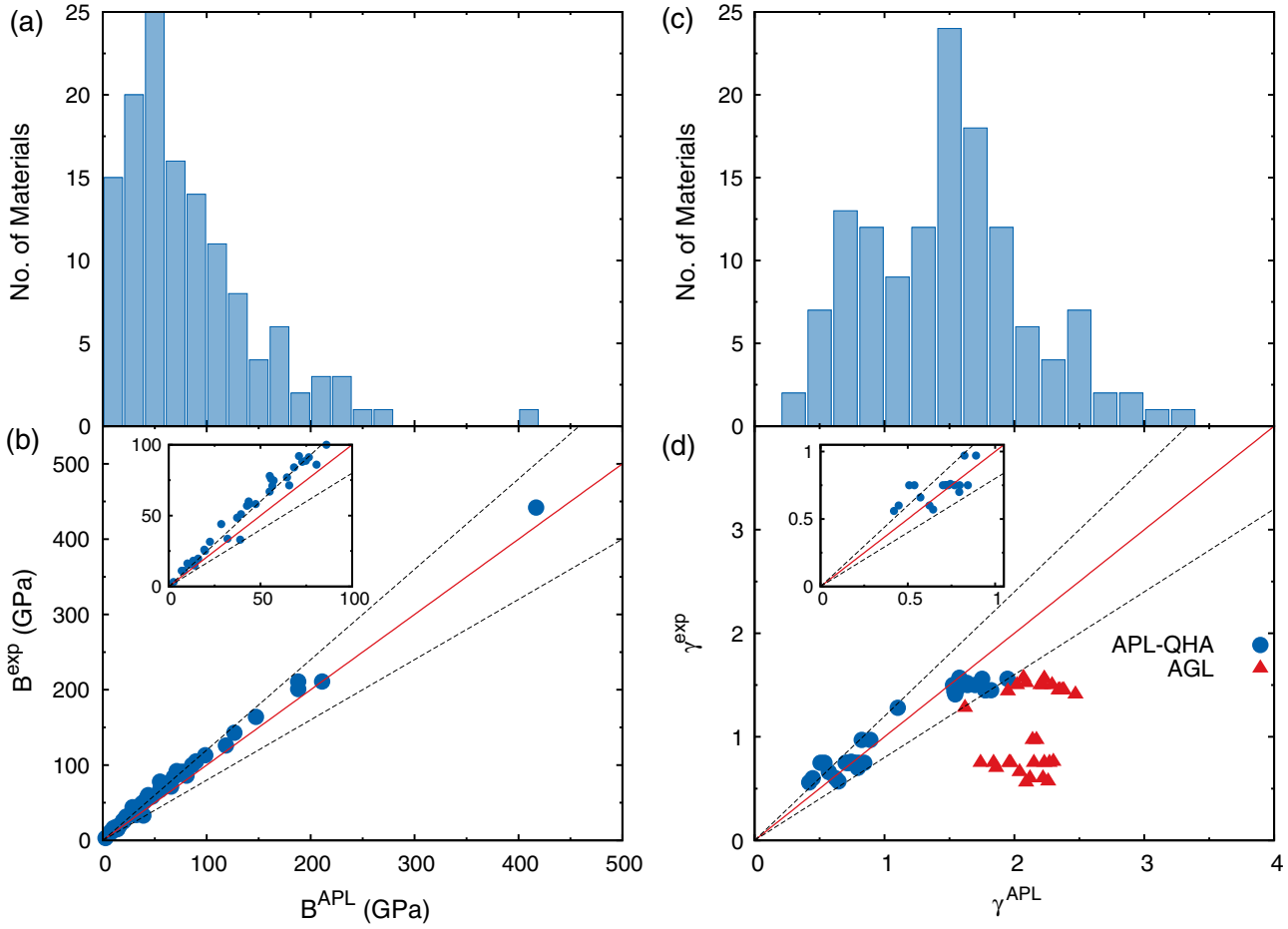

Fig. 3. (a) Histogram for the dispersion of predicted B at 300 K for the selected set of systems. (b) Comparison of experimental B^{exp} and predicted B^{APL} for the selected set of systems. The red line represents equality between experimental and predicted values and the dashed black lines represent ±20% error. (c) Histogram for the dispersion of predicted Grüneisen parameters at 300 K for the selected set of systems. (d) Comparison of experimental γ^{exp} and predicted γ^{APL} for the selected set of systems. The red line represents equality between experimental and predicted values and the dashed black lines represent ±20% error. The blue circles represent QHA-APL results and the red triangles correspond to AGL results [3]. (For interpretation of the references to color in this figure legend, the reader is referred to the web version of this article.)

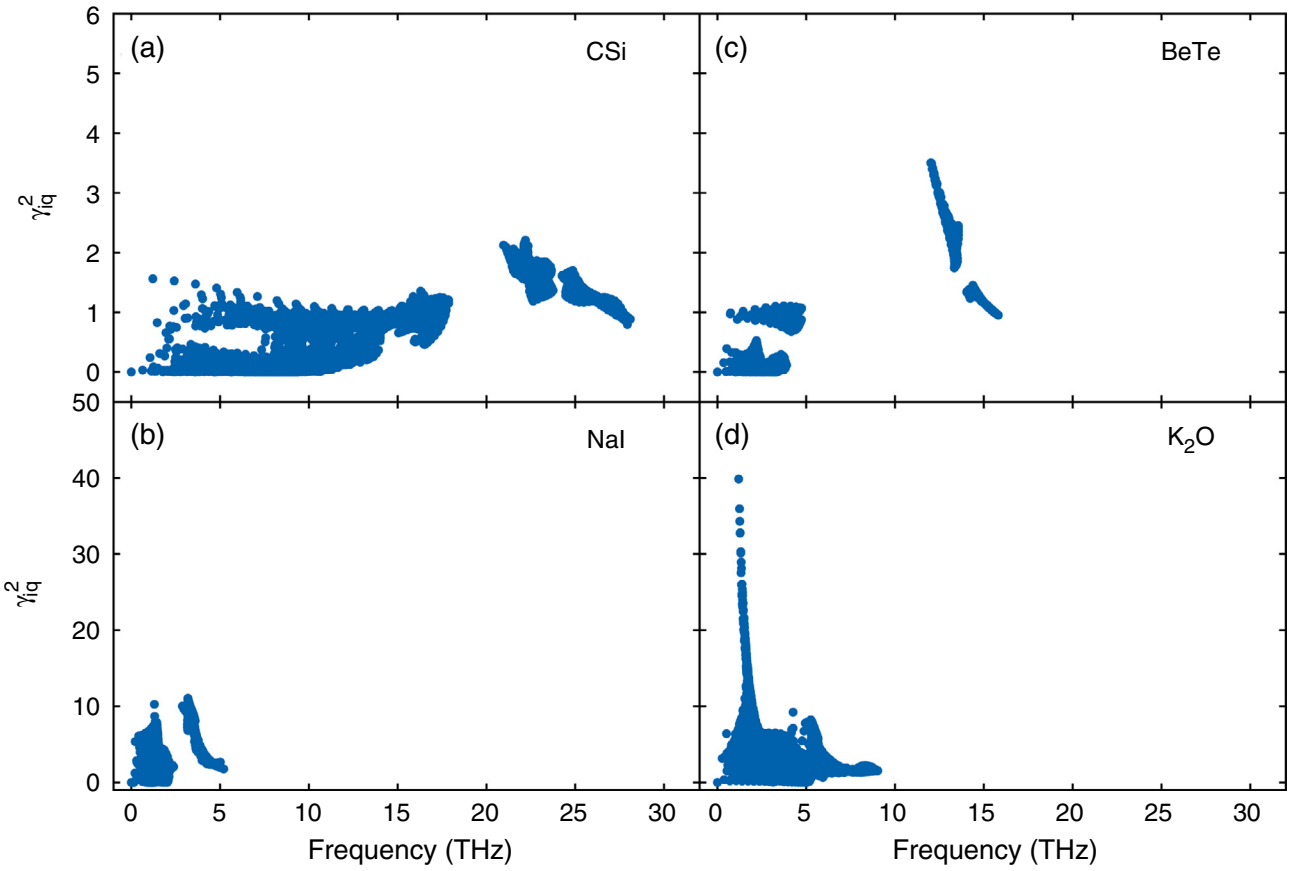

Fig. 4. Mode Grüneisen parameters for (a) CSi, (b) NaI, (c) BeTe, and (d) K_2O.

value of α below 10^{-5} K^{-1} (see Fig. 5(b)). Three of them have been already reported, C, Si and CSi. However, to the best of our knowledge, the other two materials have not been experimentally measured or predicted: MnTe and MgSe.

Isobaric specific heat, C_p, can be considered another good test for our method because of the vast amount of available experimental data (see Fig. 5(d)). The low MAD (9.84 J mol^{-1} K^{-1}) is surprising for a property in which the average value of our data set is close to 50 J mol^{-1} K^{-1}. This fact is also reflected in the relative statistical parameters (RMSrD = 6.35% and rMAX = 18.9%) and correlations close to 1.0. A caveat should be mentioned: this deviation grows slightly when comparing C_p at 1000 K instead of 300 K. This is due to higher anharmonicity at higher temperatures.

Some groups of materials are more likely to show larger deviations because of the exchange-correlation functional limitations. Inaccurate band gaps could lead to predict metallic behavior in semiconductor with a narrow band gap. This qualitative disagreement can modify the electronic terms in the free energy. To ensure that our description is correct, we have calculated the RMSrD for metals and semiconductors with a predicted band gap smaller than 1.0 eV. For metals, the RMSrD is 8.1% for C_p, which is below the RMSrD for the whole data set. We have also calculated this quantity for $\alpha_V(T)$ and C_p for low band gap semiconductors, obtaining 30.0% and 3.6% respectively. Both values are also close to the RMSrD obtained for the whole data set. Despite QHA limitations, we demonstrate that our implementation can predict the properties of different groups of materials.

We also computed the temperature dependence for selected materials in the data set (see Fig. 6). Our implementation predicts correctly the behavior of $\gamma(T)$, B, $\alpha_V(T)$ and C_p below melting points for various types of materials (metals, insulators and semiconductors). The bulk modulus for insulators such as NaCl and KCl are shown in Fig. 6(a) with errors smaller than 25%. QHA-APL also predicts $\alpha_V(T)$ for complex metals as Ni_2SnTi with a high accuracy below its melting point (see Fig. 6(b)). Finally, C_p for GaAs, a classic semiconductor, is depicted in Fig. 6(c) presenting errors smaller than 2%.

More sophisticated electronic structure methods can be used to validate our data. Our framework can use different exchange correlation functionals such as the pseudo hybrid functional ACBN0 [33]. We have used K_2O as a test to study how a more accurate functional works compared to the results obtained with PBE (see Fig. 7). Despite the use of a more accurate approach, the band gap (1.8 eV compared to 1.71 eV for PBE), phonon dispersion curves and the average Grüneisen parameter for K_2O are only slightly modified by ACBN0.

4. Conclusions

The quasi-harmonic approximation has been combined with the Automatic Phonon Library in the AFLOW high-throughput framework in order to develop a tool to accurately and robustly predict some of the most important temperature dependent properties of solids such as B, γ, α, and C_p. Lattice dynamics calculations at different volumes for fully relaxed structures are performed, managed, self-corrected, and post processed by the QHA-APL code, creating a unique workflow to populate material databases such as AFLOW. A benchmark of 130 materials has been used to test the precision and accuracy of the software. QHA-APL predicts results

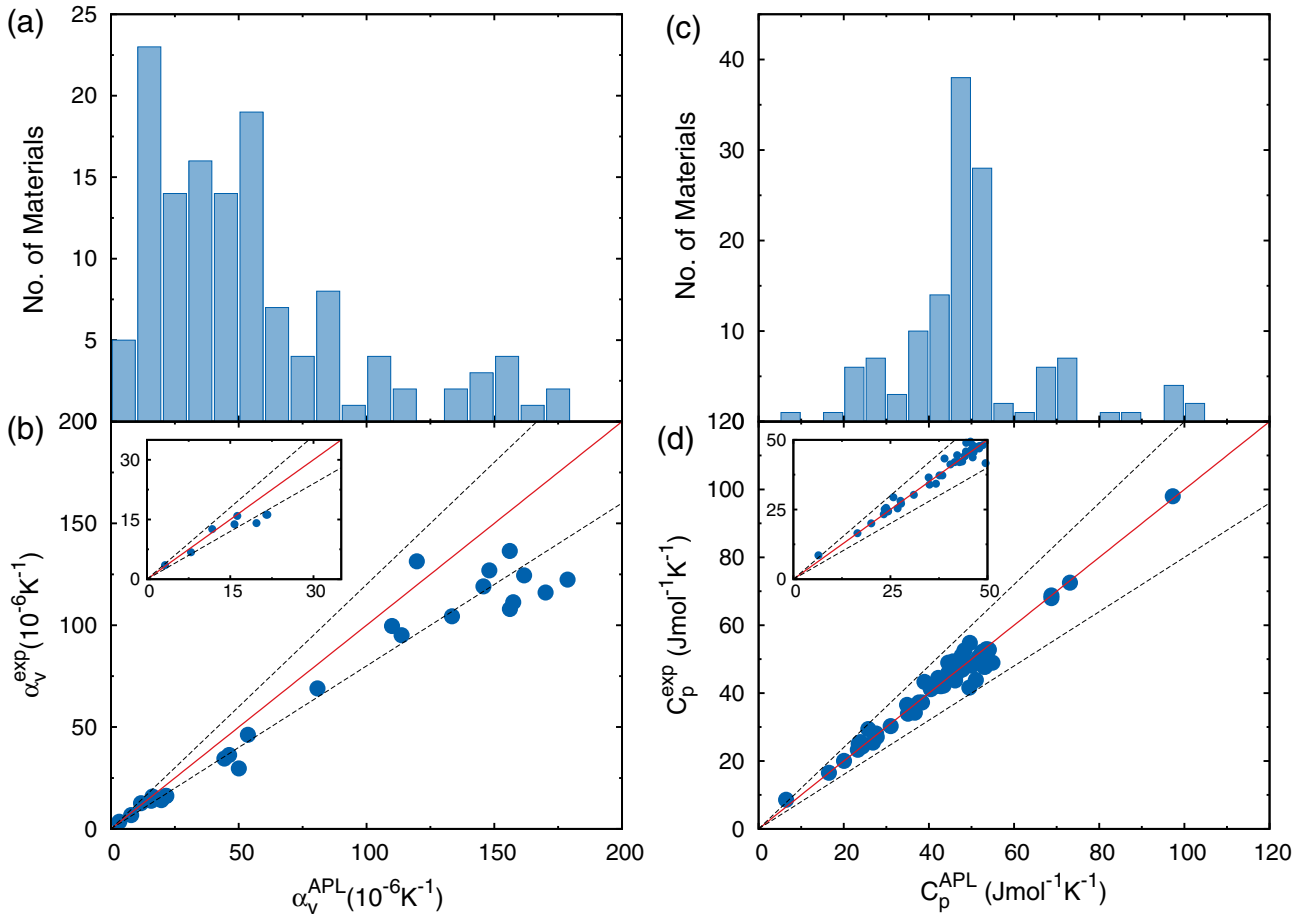

Fig. 5. (a) Histogram for the dispersion of predicted volumetric thermal expansion coefficient at 300 K for the selected set of systems. (b) Comparison of experimental α^{exp} and predicted α^{APL} for the selected set of systems. The red line represents equality between experimental and predicted values and the dashed black lines represent ±20% error. (c) Histogram for the dispersion of predicted isobaric specific heat at 300 K for the selected set of systems. (d) Comparison of experimental C_p^{exp} and predicted C_p^{APL} for the selected set of systems. The red line represents equality between experimental and predicted values and the dashed black lines represent ±20% error. (For interpretation of the references to color in this figure legend, the reader is referred to the web version of this article.)

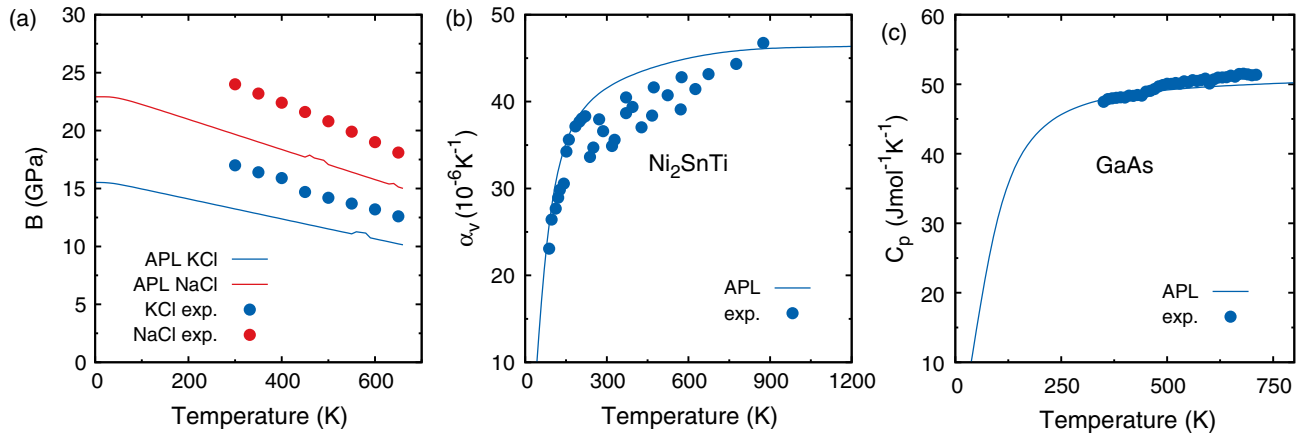

Fig. 6. (a) Predicted bulk modulus of NaCl and KCl compared to the available experimental data [63]. (b) Predicted volumetric thermal expansion coefficient of Ni_2SnTi compared to the available experimental data [64]. (c) Predicted isobaric specific heat of GaAs compared to the available experimental data [65].

whose RMSrD is below 18% for any of the four quantities with respect to experimentally reported data. We confirm recent results on K_2O and computed data for well known materials that have not been reported before. QHA-APL is useful not just for the prediction of properties for particular materials; its automation, robustness, accuracy and precision make it the perfect framework for the creation of material data sets that can be used for data mining or machine learning.

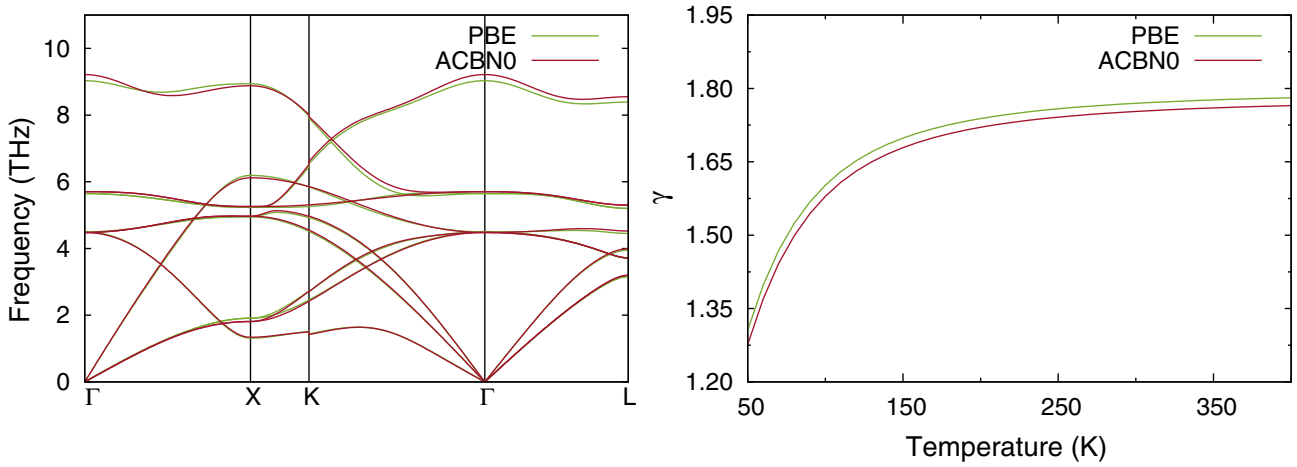

Fig. 7. (a) Phonon dispersion curves and (b) average Grüneisen parameter for K_2O using PBE and ACBN0 functionals.

Acknowledgements

We thank Dr. E. Perim, Dr. O. Levy, A. Supka, and M. Damian for various technical discussions. We would like to acknowledge support by DOD-ONR (N00014-13-1-0635, N00014-11-1-0136, N00014-09-1-0921) and by DOE (DE-AC02-05CH11231), specifically the BES program under Grant # EDCBEE. The AFLOW consortium would like to acknowledge the Duke University – Center for Materials Genomics and the CRAY corporation for computational support.

Appendix A. Supplementary material

Supplementary data associated with this article can be found, in the online version, at http://dx.doi.org/10.1016/j.commatsci.2016.07.043.

References

[1] S. Curtarolo, G.L.W. Hart, M. Buongiorno Nardelli, N. Mingo, S. Sanvito, O. Levy, The high-throughput highway to computational materials design, Nat. Mater. 12 (2013) 191–201, http://dx.doi.org/10.1038/nmat3568.
[2] M.A. Blanco, E. Francisco, V. Luaña, GIBBS: isothermal-isobaric thermodynamics of solids from energy curves using a quasi-harmonic Debye model, Comput. Phys. Commun. 158 (1) (2004) 57–72, http://dx.doi.org/10.1016/j.comphy.2003.12.001.
[3] C. Toher, J.J. Plata, O. Levy, M. de Jong, M.D. Asta, M. Buongiorno Nardelli, S. Curtarolo, High-throughput computational screening of thermal conductivity, Debye temperature and Grüneisen parameter using a quasi-harmonic Debye model, Phys. Rev. B 90 (2014) 174107, http://dx.doi.org/10.1103/PhysRevB.90.174107.
[4] W. Li, J. Carrete, N.A. Katcho, N. Mingo, ShengBTE: a solver of the Boltzmann transport equation for phonons, Comput. Phys. Commun. 185 (2014) 1747–1758, http://dx.doi.org/10.1016/j.cpc.2014.02.015.
[5] A. Togo, L. Chaput, I. Tanaka, Distributions of phonon lifetimes in Brillouin zones, Phys. Rev. B 91 (2015) 094306, http://dx.doi.org/10.1103/PhysRevB.91.094306.
[6] J.J. Plata, P. Nath, D. Usanmaz, J. Carrete, C. Toher, M. de Jong, M. Asta, M. Fornari, M. Buongiorno Nardelli, S. Curtarolo, An efficient and accurate framework for calculating lattice thermal conductivity of solids: APL2 - AFLOW Automatic Phonon Library, 2016.
[7] C.Y. Ho, R.E. Taylor (Eds.), Thermal Expansion of Solids, ASM Intl., 1998.
[8] S. Baroni, P. Giannozzi, E. Isaev, Density-functional perturbation theory for quasi-harmonic calculations, Rev. Mineral Geochem. 71 (2010) 39–57, http://dx.doi.org/10.2138/rmg.2010.71.3.
[9] P. Carrier, R. Wentzcovitch, J. Tsuchiya, First-principles prediction of crystal structures at high temperatures using the quasiharmonic approximation, Phys. Rev. B 76 (2007) 064116, http://dx.doi.org/10.1103/PhysRevB.76.064116.
[10] D. Alfé, PHON: a program to calculate phonons using the small displacement method, Comput. Phys. Commun. 180 (2009) 2622–2633, http://dx.doi.org/10.1016/j.cpc.2009.03.010.
[11] T. Duong, S. Gibbons, R. Kinra, R. Arróyave, Ab-initio approach to the electronic, structural, elastic, and finite-temperature thermodynamic properties of Ti_2AX (A = Al or Ga and X = C or N), J. Appl. Phys. 110 (2011) 093504, http://dx.doi.org/10.1063/1.3652768.
[12] J. Wang, J. Wang, A. Li, J. Li, Y. Zhou, Theoretical study on the mechanism of anisotropic thermal properties of Ti_2AlC and Cr_2AlC, J. Am. Ceram. Soc. 97 (2014) 1202–1208, http://dx.doi.org/10.1111/jace.12814.
[13] L.F. Huang, X.Z. Lu, E. Tennessen, J.M. Rondinelli, An efficient ab-initio quasiharmonic approach for the thermodynamics of solids, Comput. Mater. Sci. 120 (2016) 84–93, http://dx.doi.org/10.1016/j.commatsci.2016.04.012.
[14] A. Togo, I. Tanaka, First principles phonon calculations in materials science, Scr. Mater. 108 (2015) 1–5, http://dx.doi.org/10.1016/j.scriptamat.2015.07.021.
[15] S. Curtarolo, W. Setyawan, G.L.W. Hart, M. Jahnátek, R.V. Chepulskii, R.H. Taylor, S. Wang, J. Xue, K. Yang, O. Levy, M.J. Mehl, H.T. Stokes, D.O. Demchenko, D. Morgan, AFLOW: an automatic framework for high-throughput materials discovery, Comput. Mater. Sci. 58 (2012) 218–226, http://dx.doi.org/10.1016/j.commatsci.2012.02.005.
[16] M. Jahnátek, O. Levy, G.L.W. Hart, L.J. Nelson, R.V. Chepulskii, J. Xue, S. Curtarolo, Ordered phases in ruthenium binary alloys from high-throughput first-principles calculations, Phys. Rev. B 84 (2011) 214110, http://dx.doi.org/10.1103/PhysRevB.84.214110.
[17] L. Chaput, A. Togo, I. Tanaka, G. Hug, Phonon-phonon interactions in transition metals, Phys. Rev. B 84 (2011) 094302, http://dx.doi.org/10.1103/PhysRevB.84.094302.
[18] T. Tadano, Y. Gohda, S. Tsuneyuki, Anharmonic force constants extracted from first-principles molecular dynamics: applications to heat transfer simulations, J. Phys.: Conden. Matt. 26 (2014) 225402, http://dx.doi.org/10.1088/0953-8984/26/22/225402.
[19] S. Curtarolo, W. Setyawan, S. Wang, J. Xue, K. Yang, R.H. Taylor, L.J. Nelson, G.L.W. Hart, S. Sanvito, M. Buongiorno Nardelli, N. Mingo, O. Levy, AFLOWLIB.ORG: a distributed materials properties repository from high-throughput ab initio calculations, Comput. Mater. Sci. 58 (2012) 227–235, http://dx.doi.org/10.1016/j.commatsci.2012.02.002.
[20] R.H. Taylor, F. Rose, C. Toher, O. Levy, K. Yang, M. Buongiorno Nardelli, S. Curtarolo, A RESTful API for exchanging materials data in the AFLOWLIB.org consortium, Comput. Mater. Sci. 93 (2014) 178–192, http://dx.doi.org/10.1016/j.commatsci.2014.05.014.
[21] C.E. Calderon, J.J. Plata, C. Toher, C. Oses, O. Levy, M. Fornari, A. Natan, M.J. Mehl, G.L.W. Hart, M. Buongiorno Nardelli, S. Curtarolo, The AFLOW standard for high-throughput materials science calculations, Comput. Mater. Sci. 108 (Part A) (2015) 233–238, http://dx.doi.org/10.1016/j.commatsci.2015.07.019.
[22] D. Orlikowski, P. Söderlind, J.A. Moriarty, First-principles thermoelasticity of transition metals at high pressure: tantalum prototype in the quasiharmonic limit, Phys. Rev. B 74 (2006) 054109, http://dx.doi.org/10.1103/PhysRevB.74.054109.
[23] S. Xiang, F. Xi, Y. Bi, J. Xu, H. Geng, L. Cai, F. Jing, J. Liu, Ab initio thermodynamics beyond the quasiharmonic approximation: W as a prototype, Phys. Rev. B 81 (2010) 014301, http://dx.doi.org/10.1103/PhysRevB.81.014301.
[24] B. Grabowski, L. Ismer, T. Hickel, J. Neugebauer, Ab initio up to the melting point: anharmonicity and vacancies in aluminum, Phys. Rev. B 79 (13) (2009) 134106, http://dx.doi.org/10.1103/PhysRevB.79.134106.
[25] J.M. Skelton, S.C. Parker, A. Togo, I. Tanaka, A. Walsh, Thermal physics of the lead chalcogenides PbS, PbSe, and PbTe from first principles, Phys. Rev. B 89 (2014) 205203, http://dx.doi.org/10.1103/PhysRevB.89.205203.
[26] S. Iikubo, H. Ohtani, M. Hasebe, First-principles calculations of the specific heats of cubic carbides and nitrides, Mater. Trans. 51 (2010) 574–577, http://dx.doi.org/10.2320/matertrans.MBW200913.
[27] A. Otero-de-la Roza, V. Luaña, Treatment of first-principles data for predictive quasiharmonic thermodynamics of solids: the case of MgO, Phys. Rev. B 84 (2011) 024109, http://dx.doi.org/10.1103/PhysRevB.84.024109.

[28] T. Tohei, H.-S. Lee, Y. Ikuhara, First principles calculation of thermal expansion of carbon and boron nitrides based on quasi-harmonic approximation, Mater. Trans. 56 (2015) 1452–1456, http://dx.doi.org/10.2320/matertrans.MA201574.
[29] H. Kangarlou, A. Abdollahi, Thermodynamic properties of copper in a wide range of pressure and temperature within the quasi-harmonic approximation, Int. J. Thermophys. 35 (2014) 1501–1511, http://dx.doi.org/10.1007/s10765-014-1742-x.
[30] B.P. Burton, S. Demers, A. van de Walle, First principles phase diagram calculations for the wurtzite-structure quasibinary systems SiC-AlN, SiC-GaN and SiC-InN, J. Appl. Phys. 110 (2011) 023507, http://dx.doi.org/10.1063/1.3602149.
[31] W.J. Golumbfskie, R. Arroyave, D. Shin, Z.-K. Liu, Finite-temperature thermodynamic and vibrational properties of Al-Ni-Y compounds via first-principles calculations, Acta Mater. 54 (2006) 2291–2304, http://dx.doi.org/10.1016/j.actamat.2006.01.013.
[32] D. Wee, B. Kozinsky, B. Pavan, M. Fornari, Quasiharmonic vibrational properties of TiNiSn from ab initio phonons, J. Elec. Mat. 41 (2012) 977, http://dx.doi.org/10.1007/s11664-011-1833-4.
[33] L.A. Agapito, S. Curtarolo, M. Buongiorno Nardelli, Reformulation of DFT + *U* as a pseudohybrid hubbard density functional for accelerated materials discovery, Phys. Rev. X 5 (2015) 011006, http://dx.doi.org/10.1103/PhysRevX.5.011006.
[34] P. Giannozzi, S. Baroni, N. Bonini, M. Calandra, R. Car, C. Cavazzoni, D. Ceresoli, G.L. Chiarotti, M. Cococcioni, I. Dabo, A. Dal Corso, S. de Gironcoli, S. Fabris, G. Fratesi, R. Gebauer, U. Gerstmann, C. Gougoussis, A. Kokalj, M. Lazzeri, L. Martin-Samos, N. Marzari, F. Mauri, R. Mazzarello, S. Paolini, A. Pasquarello, L. Paulatto, C. Sbraccia, S. Scandolo, G. Sclauzero, A.P. Seitsonen, A. Smogunov, P. Umari, R.M. Wentzcovitch, QUANTUM ESPRESSO: a modular and open-source software project for quantum simulations of materials, J. Phys.: Conden. Matter 21 (39) (2009) 395502.
[35] G. Kresse, J. Hafner, Ab initio molecular dynamics for liquid metals, Phys. Rev. B 47 (1993) 558–561.
[36] D.C. Wallace, Thermodynamics of Crystals, Wiley, 1972.
[37] G.P. Srivastava, The Physics of Phonons, CRC Press, Taylor & Francis, 1990.
[38] M.T. Dove, Introduction to Lattice Dynamics, Cambridge University Press, 1993.
[39] P.E. Blöchl, Projector augmented-wave method, Phys. Rev. B 50 (1994) 17953–17979.
[40] J.P. Perdew, K. Burke, M. Ernzerhof, Generalized gradient approximation made simple, Phys. Rev. Lett. 77 (1996) 3865–3868.
[41] Y. Wang, J.J. Wang, W.Y. Wang, Z.G. Mei, S.L. Shang, L.Q. Chen, Z.K. Liu, A mixed-space approach to first-principles calculations of phonon frequencies for polar materials, J. Phys.: Condens. Matter 22 (20) (2010) 202201, http://dx.doi.org/10.1088/0953-8984/22/20/202201.
[42] W.B. Gauster, Low-temperature Grüneisen parameters for silicon and aluminum, Phys. Rev. B 4 (1971) 1288–1296, http://dx.doi.org/10.1103/PhysRevB.4.1288.
[43] W.C. Hughes, L.S. Cain, Second-order elastic constants of AgCl from 20 to 430 °C, Phys. Rev. B 53 (1996) 5174, http://dx.doi.org/10.1103/PhysRevB.53.5174.
[44] I. Barin, Thermochemical Data of Pure Substances, Wiley-VCH, 2008.
[45] O. Madelung, Semiconductors: Data Handbook, Springer Berlin Heidelberg, Berlin, 2004.
[46] G.A. Slack, The thermal conductivity of nonmetallic crystals, in: H. Ehrenreich, F. Seitz, D. Turnbull (Eds.), Solid State Physics, vol. 34, Academic, New York, 1979, p. 1.
[47] D.R. Lide, CRC Handbook of Chemistry and Physics, Taylor & Francis, 2004.
[48] D. Laplaze, M. Boissier, R. Vacher, Velocity of hypersounds in lithium hydride by spontaneous Brillouin scattering, Solid State Commun. 19 (1976) 445–446, http://dx.doi.org/10.1016/0038-1098(76)91187-X.
[49] P.K. Lam, M.L. Cohen, G. Martinez, Analytic relation between bulk moduli and lattice constants, Phys. Rev. B 35 (1987) 9190, http://dx.doi.org/10.1103/PhysRevB.35.9190.
[50] L.E. McNeil, M. Grimsditch, R.H. French, Vibrational spectroscopy of aluminum nitride, J. Am. Ceram. Soc. 76 (1993) 1132–1136, http://dx.doi.org/10.1111/j.1151-2916.1993.tb03730.x.
[51] D.T. Morelli, G.A. Slack, High lattice thermal conductivity solids, in: S.L. Shindé, J.S. Goela (Eds.), High Thermal Conductivity Materials, Springer, 2006.
[52] S. Haussühl, Thermo-elastische Konstanten der Alkalihalogenide vom NaCl-Typ, Z. für Phys. 159 (1960) 223–229, http://dx.doi.org/10.1007/BF01338349.
[53] H.H. Li, Refractive index of alkali halides and its wavelength and temperature derivatives, J. Phys. Chem. Ref. Data 5 (1976) 329–528.
[54] M. Ueno, M. Yoshida, A. Onodera, O. Shimomura, K. Takemura, Stability of the wurtzite-type structure under high pressure: GaN and InN, Phys. Rev. B 49 (1994) 14–21, http://dx.doi.org/10.1103/PhysRevB.49.14.
[55] S. Krukowski, A. Witek, J. Adamczyk, J. Jun, M. Bockowski, I. Grzegory, B. Lucznik, G. Nowak, M. Wróblewski, A. Presz, S. Gierlotka, S. Stelmach, B. Palosz, S. Porowski, P. Zinn, Thermal properties of indium nitride, J. Phys. Chem. Solids 59 (3) (1998) 289–295, http://dx.doi.org/10.1016/S0022-3697(97)00222-9.
[56] B. Xu, Q. Wang, Y. Tian, Bulk modulus for polar covalent crystals, Sci. Rep. 3 (2013) 3068, http://dx.doi.org/10.1038/srep03068.
[57] Y. Sumino, I. Ohno, T. Goto, M. Kumazawa, Measurement of elastic constants and internal frictions on single-crystal MgO by rectangular parallelepiped resonance, J. Phys. Earth 24 (1976) 263–273, http://dx.doi.org/10.4294/jpe1952.24.263.
[58] Z.P. Chang, E.K. Graham, Elastic properties of oxides in the NaCl-structure, J. Phys. Chem. Solids 38 (1977) 1355–1362, http://dx.doi.org/10.1016/0022-3697(77)90007-5.
[59] J. Carrete, W. Li, N. Mingo, S. Wang, S. Curtarolo, Finding unprecedentedly low-thermal-conductivity half-Heusler semiconductors via high-throughput materials modeling, Phys. Rev. X 4 (2014) 011019, http://dx.doi.org/10.1103/PhysRevX.4.011019.
[60] A.E. Gheribi, A. Seifitokaldani, P. Wu, P. Chartrand, An ab initio method for the prediction of the lattice thermal transport properties of oxide systems: case study of Li_2O and K_2O, J. Appl. Phys. 118 (2015) 145101, http://dx.doi.org/10.1063/1.4932643.
[61] R. Al Rahal Al Orabi, N.A. Mecholsky, J. Hwang, W. Kim, J.-S. Rhyee, D. Wee, M. Fornari, Band Degeneracy, Low thermal conductivity, and high thermoelectric figure of merit in SnTe-CaTe alloy, Chem. Mater. 28 (2016) 376–384, http://dx.doi.org/10.1021/acs.chemmater.5b04365.
[62] P. Vaqueiro, R. Al Rahal Al Orabi, S.D.N. Luu, G. Guélou, A.V. Powell, R.I. Smith, J.-P. Song, D. Wee, M. Fornari, The role of copper in the thermal conductivity of thermoelectric oxychalcogenides: do lone pairs matter?, Phys Chem. Chem. Phys. 17 (2015) 31735, http://dx.doi.org/10.1039/C5CP06192J.
[63] S.K. Srivastava, P. Sinha, M. Panwar, Thermal expansivity and isothermal bulk modulus of ionic materials at high temperatures, Ind. J. Pure Appl. Phys. 47 (2009) 175–179.
[64] P. Hermet, R.M. Ayral, E. Theron, P.G. Yot, F. Salles, M. Tillard, P. Jund, Thermal expansion of Ni-Ti-Sn Heusler and half-Heusler materials from first-principles calculations and experiments, J. Phys. Chem. C 118 (39) (2014) 22405–22411, http://dx.doi.org/10.1021/jp502112f.
[65] J.S. Blakemore, Semiconducting and other major properties of gallium arsenide, J. Appl. Phys. 53 (1982) R123–R181, http://dx.doi.org/10.1063/1.331665.